# Establishing the Relationship Between Manufacturing and Component Performance in Stretch Formed Thermoplastic Composites

Michael H. Santare, R. Byron Pipes,
A. J. Beaussart, D. W. Coffin, B. J. O'Toole, S. F. Shuler

Department of Mechanical Engineering and
Center for Composite Materials
University of Delaware

Flexible manufacturing methods are needed to reduce the cost of using advanced composites in structural applications. One method that allows for this is the stretch forming of long discontinuous fiber materials with thermoplastic matrices. In order to exploit this flexibility in an economical way, a thorough understanding of the relationship between manufacturing and component performance must be developed. This paper reviews some of the recent work geared toward establishing this understanding. Micromechanics models have been developed to predict the formability of the material during processing. The latest improvement of these models includes the viscoelastic nature of the matrix and comparison with experimental data. A finite element scheme is described which can be used to model the forming process. This model uses equivalent anisotropic viscosities from the micromechanics models and predicts the microstructure in the formed part. In addition, structural models have been built to account for the material property gradients that can result from the manufacturing procedures. Recent developments in this area include the analysis of stress concentrations and a failure model each accounting for the heterogeneous material fields.

## Motivation

The extraordinary properties of collimated fiber composites consisting of continuous fibers suspended in polymeric matrices have been widely acclaimed during the past two decades. These materials were made possible by the invention of synthetic fibers which possess specific strengths significantly greater than conventional monolithic materials. The recent introduction of thermoplastic polymer matrices now offers the potential to develop manufacturing methods for these new composite materials that can take advantage of lower cost conventional manufacturing methods.

Sheet forming of metallic materials is one of the most pervasive manufacturing methods in the contemporary manufacturing technology. However, unlike monolithic metallic sheet, continuous fiber composites possess direction of inextensibility in the fiber direction. For these material systems the dominant modes of deformation during sheet forming are shearing. Extensibility in the fiber direction can, however, be provided by introducing breaks along the fiber length so that the individual fibers are made discontinuous [1]. The development of extensibility in the fiber direction for the collimated fiber composite results in enhanced formability of multiaxial sheet products.

The objective of the present work is to develop the science base for a series of models that can be used to link manufacturing with structural performance. This is shown schematically in Figure 1.

## Micromechanics Analysis

The primary objective of the micromechanics analysis is to develop relationships between the primary anisotropic viscosities, $\eta_{ij}$ and the properties of the oriented fiber assembly and matrix fluid. There have been many studies of the flow of dilute suspensions of fibers and particles in

liquids, for example by Metzner [2] and recently Rogers [3]. The micromechanical analysis presented here, however, addresses a collimated, discontinuous fiber assembly suspended in a viscous matrix fluid which is subjected to relatively small total strains.

Consider an aligned fiber assembly wherein long discontinuous and rigid fibers are arranged in a regular cross-sectional geometry (hexagonal or square array) and suspended in a viscous fluid (Figure 2). At the interface between the fibers and matrix fluid, a no slip condition is assumed. In addition, it is assumed that neighboring fibers can be treated as if they were arranged so that fiber ends in one row are next to fiber centers in adjacent rows. This geometry is possible for a square array, but not for a hexagonal array, where the assumption must be regarded as a simplifying approximation.

## Fiber Array Geometric Relations

Consider the geometric arrangements of fibers. For fibers of diameter, $D$, and arranged in a fixed pattern where the spacing between fibers, $S$, then the fiber volume fraction, $f$, is given as:

$$f = F \left(\frac{D}{S}\right)^2 \quad \text{where } F = \begin{cases} \dfrac{\pi}{2\sqrt{3}} & \text{(hexagonal array)} \\ \dfrac{\pi}{4} & \text{(square array)} \end{cases} \tag{1}$$

The following fiber volume fraction parameter is now introduced:

$$\kappa = \frac{1}{1 - \sqrt{f/F}} \tag{2}$$

## Effective Viscosities of Oriented fiber Assembly Newtonian Matrix Fluids

If a linear variation in velocity in the direction of the fibers is imposed upon the oriented fiber assembly, the relative velocity of adjacent fibers may be determined by assuming that the fibers travel at the velocity of their centroids (Figure 3). Hence, the relative velocity of two adjacent fibers of length L is given as,

$$\Delta \dot{u} = \dot{\varepsilon}_1 L/2 \tag{3}$$

where $\dot{\varepsilon}_1$ is the extensional strain rate of the fiber assemblage. Therefore the apparent shear strain rate in the fluid contained between the nearest points of two adjacent fibers is

$$\dot{\gamma} = \frac{(L/D) [\kappa - 1] \dot{\varepsilon}_1}{2} \tag{4}$$

The induced shearing strain rate, $\dot{\gamma}$, generates a shearing stress, $\tau$, on the fiber surfaces equal to the product of the fluid shear viscosity, $\eta$, and the strain rate, $\eta\dot{\gamma}$. At a cross-section through the fiber midpoints, half of the fibers will carry the total load, and so the fiber tensile stress at the midpoint will be $2\sigma/f$, where $\sigma$ is the average stress in the system. This force equilibrium implies that the tensile force at the fiber midpoint must equal the total surface shear force over a length $L/2$. This results in the following equation,

572

$$\tau = \frac{\sigma}{f} (D/L) \qquad (5)$$

Combining Equations (1-5) yields the expression for the elongational viscosity, $\eta_{11}$, as listed in Table 1.

In order to develop simple relations for the effective shearing viscosities, the fibers are again assumed to behave rigidly and a no slip condition is assumed at the fluid fiber interface. By imposing pure steady state shearing motion, the shearing strain rate of the matrix fluid can be geometrically related to the effective shearing strain rate of the fiber-fluid unit cell. For a Newtonian viscous fluid the shear stress is related to the fluid strain by $\tau = \eta \dot{\gamma}$. This leads to the Newtonian expressions for $\eta_{12}$ and $\eta_{13}$ listed in Table 1.

Following the development for the effective transverse shearing viscosity, $\eta_{23}$, the effective transverse elongational viscosity, $\eta_{22}$, may be determined (for $\eta_{11} >> \eta_{22}$) and is listed again in Table 1.

## Power-Law Matrix Fluids

The previous relationships have all been developed assuming a matrix fluid which follows Newtonian behavior. Consider next the constitutive relations for a matrix fluid which takes the non-Newtonian form of a simple power-law with yield stress, $\tau_o$:

$$\tau = \eta \dot{\gamma}^m + \tau_o \qquad (6)$$

Incorporating this expression, the anisotropic viscosities for the assembly with power-law fluid can be developed. (See Table 1.)

## Carreau Model Matrix Fluids

A deficiency of the simple power-law constitutive relation for a shear thinning fluid is its lack of a finite zero-shear viscosity. Carreau [4] has introduced the following empirical rheological model to describe the non-Newtonian behavior of such a fluid:

$$\eta = \bar{\eta}_0 [ 1 + (\bar{\lambda} \dot{\gamma})^2 ]^{(n-1)/2} \qquad (7)$$

Where $\bar{\eta}_0 = \eta_0 A_T$, $\bar{\lambda} = \lambda A_T$ with the temperature shift factor $A_T = \exp \xi[(T_0-T)/T]$. The parameters $\eta_0$, $\lambda$, n and $\xi$ are determined empirically. The onset of non-linearity is determined by the time constant $\bar{\lambda}$ and the exponent n determines the degree of non-linearity. The value n=1 corresponds to a Newtonian fluid and as n decreases the fluid exhibits increased shear thinning. Employing this matrix constitutive relation and again assuming a linear velocity gradient for the

matrix fluid, it is possible to derive new expressions for effective viscosities of the medium as listed in Table 1.

## Comparison of Predicted Viscosities to Experimentally Obtained Data

Binding [5] has measured the shearing viscosity versus strain rate for neat polypropylene at 200°C. Employing a least squares approximation, the Carreau equation was fit to the Binding data and the Carreau parameters were determined. A comparison between the Binding data and the Carreau model prediction is shown in Figure 4.

Binding also measured the elongational and shear viscosities of a 25 volume percent glass fiber/polypropylene melt (200°C) suspension utilizing a converging flow orifice die and a capillary die, respectively. When the parameters determined from the curve fit above are combined with the Carreau equations from Table 1, the elongational and shearing viscosities of the glass fiber/polypropylene suspension can be predicted as a function of strain rate. The measured and predicted elongational viscosities of the polypropylene/glass suspension as a function of strain rate are shown in Figure 5. The model predictions shown in Figure 5 correspond to a maximum fiber packing fraction, F, of 0.846 (an average of square and hexagonal array values).

Binding noted that the average fiber aspect ratio of the suspension was 588 prior to the test. Due to fiber breakage which occurred during the flow the post-extrusion fiber aspect ratio was approximately 200. The two predictions for L/D of 588 and 200 bound the data.

The shear rate in the matrix fluid is amplified by the presence of the fibers. For the range in elongational rates of $10^0$ to $10^2$ s$^{-1}$ in this suspension, the corresponding shear rate in the matrix fluid viscosity is $10^2$ to $10^4$ s$^{-1}$. To achieve a better description of the matrix fluid viscosity in the $10^2$ to $10^4$ s$^{-1}$ shear rate range, a new set of Carreau parameters were chosen.

A summary of the predictions for the anisotropic viscosities of the suspension are shown in Figure 6. Several observations should be made regarding these predictions. First, the prediction for an average aspect ratio (L/D) of 360 shows excellent agreement with the Binding Data. Second, at low shear rates, the elongational viscosity, $\eta_{11}$, is approximately $10^4$ Pa-s greater than the shearing viscosities of the suspension.

The agreement between the developed relations and the Binding data offer strong support for their validity. This ability to predict the effective viscosities of anisotropic thermoplastic sheet materials by knowing the rheological behavior of only the matrix polymer should prove valuable in the sheet forming technology.

## Review of Finite Element Analysis for Forming Processes

Thermoforming of advanced thermoplastic composites has many similarities to metal sheet forming technology. The use of computer-aided techniques in the metal-forming industry has increased considerably in the last several years. The finite element method has become a common tool for the simulation of sheet metal forming processes. The analysis provides useful information about the forming rates, stress and strain distributions. They are also helpful in predicting optimum process conditions and in designing dies and equipment.

The first approach to analyze a metal-forming process is to treat the metal as a deformable solid and to use the displacements as the primary variables. This solid mechanics approach is based on the use of elasto-plastic models.

Elastic effects can be neglected in most metal-forming processes where large, permanent deformations occur. For such cases, a viscoplastic model is adopted to describe the behavior of the deforming material. A general numerical finite-element solution was presented in 1979 by Zienkiewicz and Godbole for viscoplastic materials [6]. This second approach is usually referred to as the flow formulation for forming processes. In this technique, the material is treated as a viscous medium and the velocities are the primary variables. Since the behavior of the composite system at its forming temperature is described in the present work by the constitutive equation for a

574

viscous, anisotropic medium, it is thus logical to apply the flow formulation to this material. The high degree of anisotropy must be, however, taken into account.

In the flow formulation, the finite element discretization is attained using an analogy with solid mechanics [7] that will be summarized briefly here. The equilibrium equation for an elastic solid is also valid for a viscous medium if dynamic effects are neglected. This is the case for relatively slow forming processes.

In fluid mechanics, the strain-rates are defined by the spatial derivatives of the velocity, v:

$$\dot{\varepsilon}_{ij} = \frac{1}{2} \left( \frac{\partial v_i}{\partial x_j} + \frac{\partial v_j}{\partial x_i} \right) \tag{8}$$

This expression is similar to that of strains in the solid mechanics formulation for small deformation problems.

$$\varepsilon_{ij} = \frac{1}{2} \left( \frac{\partial u_i}{\partial x_j} + \frac{\partial u_j}{\partial x_i} \right) \tag{9}$$

where u is the displacement.

The constitutive equation for a non-Newtonian viscous fluid is used to describe viscoplastic materials. It can be expressed as

$$\dot{\varepsilon}_{ij} = \frac{1}{2\mu} (\sigma_{ij} - \delta_{ij}P) \tag{10}$$

where P is the pressure term and $\mu$ is the viscosity of the medium. For incompressible elasticity, the constitutive equation can be written in the following form:

$$\varepsilon_{ij} = \frac{1}{2G} (\sigma_{ij} - \delta_{ij}P) \tag{11}$$

The constitutive relationships 10 and 11 have an identical form. There is thus an analogy between incompressible elasticity and creeping flow problems. This analogy allows the adaptation of the finite element technique and programs used in elasticity for viscous flow problems [7]. Strains are simply replaced by strain-rates, displacements by velocities, and the elastic shear modulus G by viscosity, $\mu$.

## Numerical Modeling for Thermoplastic Composites

The flow formulation briefly described in the previous section can be combined with the plane stress assumption to model forming processes of thin sheets with plate or shell finite elements. This combination was first introduced in 1983 by Onate and Zienkiewicz [8] in their viscous shell model for metal sheet-forming. In this technique, the constitutive equation for a creeping flow is simplified by the plane stress assumption as in shell theory. Large deformations of viscoplastic sheets are then studied as a series of small deflection steps, each being analogous to a small deformation elastic problem. These authors restricted their study to isotropic metals although they mentioned the validity of their method for anisotropic materials if the rotation of the principal axes of anisotropy is considered.

The constitutive relations introduced in the previous sections are adapted in the present study to perform a finite element analysis derived from the method introduced for sheet metal forming. The following scheme is proposed:

1. Solve for the velocity field "V" in the initial geometry using analogy to elasticity;
2. Update the geometry by "V∆t" where ∆t is an appropriate time step;
3. Update the sheet thickness using the incompressibility condition;
4. Update the local fiber orientations;
5. Change the boundary conditions if new points come into contact with a mold surface;
6. Repeat the procedure for the new configuration.

An independent problem is solved at each stage of the deformation in a given configuration. This approximation is reasonable if the time step ∆t is chosen so as to limit the displacements to small values. Each stage corresponds then to a small deformation elastic problem. Very large deformations can be followed with this procedure. However, the updating of the mesh may lead to mesh distortion and it may be therefore necessary to redefine the mesh at some point. It should be also noted here that at the present time the problem solved at each stage of the deformation is linear. However, the non-linear constitutive relations may be adapted. An iterative technique is then used at each stage of the solution scheme, as is the case of viscoplastic metals.

## 2-D Plane Stress Model

The applicability of the flow approach to the case of highly anisotropic materials has been first studied with a 2-D plane stress finite-element code. To take into account the fiber orientation change during the deformation, a vector is associated in this model with each element and represents the local fiber orientation. Because of the high fiber volume ratio, it is reasonable to assume that the fiber orientation moves as a material line. The displacement of the orientation vector is computed after each time step by analogy with elasticity. Consider the vector F denoting the fiber orientation in the mth element. F forms an angle $\theta$ with the x-axis of the global referential frame in the initial geometry. The components of F are given after a time-step ∆t by:

$$F_x' = \cos\theta_m + \dot{\varepsilon}_x \Delta t \cos\theta_m + \dot{\varepsilon}_{xy} \Delta t \sin\theta_m - \dot{\omega}_{xy} \Delta t \sin\theta_m \qquad (12)$$

$$F_y' = \sin\theta_m + \dot{\varepsilon}_{xy} \Delta t \cos\theta_m + \dot{\varepsilon}_y \Delta t \sin\theta_m + \dot{\omega}_{xy} \Delta t \sin\theta_m \qquad (13)$$

where

$$\dot{\varepsilon}_x = \frac{\partial U}{\partial x} \qquad\qquad \dot{\varepsilon}_y = \frac{\partial V}{\partial y}$$

$$\dot{\varepsilon}_{xy} = \frac{1}{2}\left(\frac{\partial V}{\partial x} + \frac{\partial U}{\partial y}\right) \qquad\qquad \dot{\omega}_{xy} = \frac{1}{2}\left(\frac{\partial V}{\partial x} - \frac{\partial U}{\partial y}\right)$$

The velocity field is denoted by U and V in this case. The rotation term $\dot{\omega}_{xy}$ is computed numerically in the same way as the strain rates by using the derivatives of the velocities modeled with the shape functions.

The simulation of an off-axis tensile test for a viscous fiber assembly illustrates well this 2-D model. Figure 7 shows the initial geometry of this example. The initial fiber orientation is 45 degrees. The following theoretical properties are employed: $\eta_{11} = 20\eta_{22}$ and $\eta_{22} = 3\eta_{12}$. The

576

element chosen here is a nine-node quadratic element with nine integration points. The mesh has 16 elements, and the time step is 2.5 sec. A normal velocity of 1 sec$^{-1}$ is applied to the edge 2-3. The edge 1-4 is clamped. The deformed geometry at different stages is shown in Figure 8. Note that each element is divided in four parts in that figure. The fiber orientation at the center of each element is presented in Figure 9. The fiber orientation varies between 25 and 40 degrees in the geometry obtained after 50 percent of elongation. Although the mesh is quite coarse, this simple example shows clearly the importance of taking into account the fiber rotation during the deformation in the numerical model. The simulation of the web of a curved beam in a thermoforming process and the extension of the present model to the use of continuous fiber systems are discussed in reference [9].

## Structural Analysis of Manufactured Components

Manufacturing processes such as sheet forming and stretch forming can be used to produce a variety of composite parts. The use of a long discontinuous fiber material system allows for material stretching over complex curvature parts while maintaining a high percentage of the continuous fiber material properties [10]. Combination of these forming methods and material system allows the production of complex structures such as curved beams as shown in Figure 10. The microstructure of a curved beam is sensitive to the production method and gradients in material properties are expected in both sheet formed [11] and stretch formed [12] beams. Schematic examples of two types of heterogeneity are shown in Figure 11; analysis of these types of beams can be useful in determining the effect of such property gradients on the overall performance of a given beam.

In the following section, the results of two separate analyses are reviewed. The first uses a closed form stress potential approach [13] to investigate the effect of radial heterogeneity on curved beams loaded in pure bending. The stress state is found for beams which can have several different geometries including I, J, T, and rectangular cross-sections. Material properties can be specified independently for each section of the beam, i.e., flange and web can have different properties. Each section of the beam is treated as an individual curved rectangular beam loaded in pure bending and with a constant distributed load on the curved surfaces. Superposition is used to combine the results of the individual sections into the total beam solution. Details of the analysis are provided in reference [11]. Results are shown for comparison with known solutions.

The second analysis technique uses a Rayleigh-Ritz approach [14] to solve the minimum potential energy equation for several curved beam problems including pure bending and a beam with a uniform distributed load. This is an approximate solution which uses an assumed series formulation of the displacement field. The advantage of this method is that it allows for any type of material heterogeneity and can be used to solve other relevant problems such as tensile loaded beams or beams with geometric stress concentrations such as cutouts.

Analysis results have been compared to solutions found by using mechanics of materials and finite element methods. The mechanics of materials solutions are useful for comparing results for beams with homogeneous material properties and the finite element analysis is necessary to solve the problem when the beam has heterogeneous material properties. The first type of analysis has been incorporated into a design tool for analyzing curved beams loaded in pure bending. A wide range of geometric parameters and material properties can be analyzed with relative ease. The second type of analysis is being developed so that a similar tool can be used to analyze curved beams with different loading conditions or geometric configurations.

## Results of Structural Analysis

The superposition model, which is used to find stresses and displacements in a curved beam loaded in pure bending, has been verified by comparing results with mechanics of materials and finite element analysis solutions. Several example problems of isotropic beams having I-, T-, or rectangular cross-sections have been examined and the difference between the superposition and

mechanics of materials solutions is less than 1% for all cases. Two-dimensional finite element analysis is used to compare results for a curved heterogeneous anisotropic J-beam. The heterogeneity is introduced into the finite element analysis by varying the material properties in each element of the model.

The validity of the model has been demonstrated and the effect of radial heterogeneity on beam performance can now be determined. The maximum tangential stress and maximum displacement versus heterogeneity are found for a curved J-beam loaded in pure bending. The degree of heterogeneity is varied from approximately a 20% decrease to a 20% increase in stiffness along the radial dimension. The effect of material heterogeneity is highly dependent on the beam geometry which is characterized by the average radius to depth ratio, $R/t$. Heterogeneity has a considerable effect on the maximum tangential stress in beams with a small radius of curvature, $R/t = 1$, while it has virtually no effect on the stresses in beams with a large radius of curvature. The maximum displacement is effected by heterogeneity for all beam geometries considered, but, the effect is again seen more drastically in beams with small curvature.

The Rayleigh-Ritz technique is used to solve the problem of a curved beam loaded by internal and external pressure. Solutions are compared with exact results for isotropic and axisymmetric anisotropic beams [13], and the difference is within 0.1%. This solution technique is also verified by solving the problem of an infinite plate with a centrally located hole loaded only by an internal pressure where the principle material directions are along the Cartesian axes. This problem is modeled by letting $r_i = 2.54$ cm, $r_o = 76$ cm, $P_i = 1$ Pa, and $P_o = 0$ Pa. The stress concentrations found at $\theta = 0°$ and $90°$ are within 1% of those found by Lekhnitskii, [13]. A carbon reinforced thermoplastic composite ring with an inner radius of 15.2 cm and an outer radius of 20.3 cm is analyzed for two different fiber arrangements, one with tangentially oriented fibers and the second with fibers aligned in the x-direction. The stress distribution is axisymmetric in the ring with tangentially oriented fibers as shown in Figure 12a while the ring with straight fibers in the x-direction has a slight stress concentration at approximately $\theta = 45°$ as shown in Figure 12b. These results are evidence that the tangential heterogeneity due to non-axisymmetric fiber distribution can effect the stresses in a curved beam loaded by internal and external pressure.

The Rayleigh-Ritz technique is also used to solve the problem of a curved beam loaded in pure bending. Results for isotropic beams compare to within 1% of the elasticity solutions. Results for anisotropic beams with the principle fiber directions along the polar axes also compare to within 1%. The results for beams having heterogeneous material properties are currently being compared to finite element analysis solutions.

## Introduction To Notched Composites Failure Theories

The tensile failure of notched composite plates has been studied by many researchers. Waddoups, et al. [15] applied linear elastic fracture mechanics to notched composites. They assumed an intense energy region to exist at the hole which is represented by a characteristic length, 'a'. A crack of length 'a' is used to represent this region and the stress intensity factor, $K_1$, is used to predict the notched strength. A parametric study is conducted to determine the effect of 'a' and find which value best represents experimental data.

Nuismer, et al. [16-19], used similar methods known as the point and average stress criteria. These methods use the stress distribution for an infinite plate with a circular hole subject to uniaxial tension. A stress concentration of 3 is obtained for all hole sizes, but the stress intense region is very localized for smaller holes. A larger volume of material is subject to a concentrated stress for plates with a larger hole. Experimental results verify that plates with larger holes have a smaller fracture stress. The point stress criteria assumes that the notched strength is obtained when the stress at a certain distance away from the hole edge, $d_0$, reaches the unnotched strength. The average stress criterion assumes that the notched strength is obtained when the average of the stress over a certain distance in front of the hole, $a_0$, reaches the unnotched strength.

These methods and several others not mentioned are empirical failure theories. They rely on some parameter which has to be chosen so that the theory matches the experimental data. They

**578**

can not be determined from basic material data. Backlund [20] developed the fictitious crack model, which only uses fundamental material parameters such as stiffnesses, unnotched strength $\sigma_0$, and fracture energy $G_c$, to predict the notched strength of composites. The fracture energy, $G_c$, is used to represent all the micromechanical fracture mechanisms and damage accumulating in the stress intense region at the edge of the notch. Backlund and Aronsson [21, 22] use this method to model the entire crack formation process. The failure load can also be determined for various shapes of notches.

## The Fictitious Crack Model

The basic principle of this method is to model all of the microcracks and local fractures as one fictitious crack with closing stresses acting on its surfaces as shown in Figure 13. The fictitious crack is formed when the unnotched tensile strength $s_0$ of the material is exceeded. The crack opening, 2v, increases as the load is increased and the closing stresses are reduced. The relationship between this stress and the crack opening is shown in Figure 14. The stress at the tip of the crack is always equal to the unnotched fracture stress and the closing stress is assumed to be a linearly decreasing function of the crack opening, 2v. The area under the s -v curve is equal to the fracture energy, $G_c$. The closing stress is reduced to zero at a limiting value of the crack opening, $v_c$, and at this point a real crack is assumed to form. Backlund and Aronsson studied several different functional relations between s and v; the linear relation provided the best approximation to experimental data. The applied load is increased and the crack grows in a stable manner at first and after a critical load it begins to grow in an unstable manner. This critical load is taken as the failure load.

## The Numerical Technique

The fictitious crack failure prediction is carried out using finite element analysis. The problem of a rectangular plate with a circular hole is used as an example. Only a quarter of the plate needs to be analyzed due to symmetry and the crack path is assumed to be horizontal as shown in Figure 15. The external load is introduced into the plate by a displacement, d. A stiffness matrix relating external displacement d and crack openings $v_i$ to external load P and crack surface loads $F_i$ is obtained using finite element analysis as shown in Equation 14.

$$
\begin{bmatrix} P \\ F_1 \\ F_2 \\ F_3 \\ F_4 \\ F_5 \end{bmatrix} = \begin{bmatrix} k_{11} & k_{12} & k_{13} & k_{14} & k_{15} \\ k_{21} & k_{22} & k_{23} & k_{24} & k_{25} \\ k_{31} & k_{32} & k_{33} & k_{34} & k_{35} \\ k_{41} & k_{42} & k_{43} & k_{44} & k_{45} \\ k_{51} & k_{51} & k_{51} & k_{51} & k_{55} \\ k_{61} & k_{61} & k_{61} & k_{61} & k_{65} \end{bmatrix} \begin{bmatrix} d \\ v_1 \\ v_2 \\ v_3 \\ v_4 \end{bmatrix}
\tag{14}
$$

All of the crack openings, $v_i$, are initially set equal to zero representing the undamaged plate. The initiation of damage occurs when the stress at node 1 is equal to the unnotched strength, $s_0$. The corresponding nodal force, $F_1$, is taken as ($\sigma_0$ b t)/2, where b is the distance between nodes and t is the plate thickness. The external displacement which causes this initiation of damage is found from the second row of equation 1, $d^1 = F_1/k_{21}$ and the corresponding external load is found from row 1, $P^1 = F_1 k_{11}/k_{21}$.

The next step is to allow the crack to open at node 1 and to calculate the external load which makes $F_2 = (\sigma_o \, b \, t)$. Equation 1 can be simplified as shown below since $v_2$, $v_3$, and $v_4$ are equal to zero.

$$\begin{bmatrix} P^2 \\ F_1 \\ \sigma_o \, b \, t \end{bmatrix} = \begin{bmatrix} k_{11} & k_{12} \\ k_{21} & k_{22} \\ k_{31} & k_{32} \end{bmatrix} \begin{bmatrix} d^2 \\ v_1 \end{bmatrix} \qquad (15)$$

The relationship between $F_1$ and $v_1$ is known from the assumed linear function in Figure 14, $F_1 = (\sigma_o \, b \, t)/2(1 - v_1/v_c)$. Therefore the second two rows of Equation 15 can be solved simultaneously for the two unknowns $d^2$ and $v_1$. The corresponding external load $P^2$ is then determined from row 1. This procedure is repeated by increasing the crack length by one node at each step.

By coupling this damage zone model with the structural analyses described previously, a failure prediction model for heterogeneous structures can be developed. This work is currently underway.

## Conclusions

The effective viscosities were shown to be functions of the fiber aspect ratio, the fiber volume fraction, and the matrix fluid shearing viscosity. The elongational viscosity of the suspension was found to vary as the square of the fiber aspect ratio while the shearing viscosities of the suspension were not related to fiber aspect ratio. All the anisotropic viscosities showed a complex relationship to fiber volume fraction. For a Newtonian fluid, the effective shearing viscosity of the fiber filled fluid can be related to the matrix viscosity through the factor $\kappa$, which depends only on the fiber volume fraction and packing geometry. However, the shearing viscosities of many polymeric fluids exhibit Newtonian behavior at low strain rates and power-law behavior at higher strain rates. Consequently, relations were needed for suspensions in which the matrix fluid exhibited non-Newtonian shear thinning behavior. This has been accomplished by considering an assembly of fibers suspended in a power-law fluid with finite yield stress. The relations for predicting the effective viscosities were then extended to include zero-shear viscosity and temperature dependance through incorporating the Carreau model into the existing relations.

The numerical analysis for sheet forming of long, discontinuous fiber reinforced thermoplastics has been investigated in this research. These materials are modeled at their forming temperature as a highly anisotropic, viscous medium. This study demonstrates that a finite element technique developed for the simulation of metal sheet forming processes can be adapted to the case of advanced thermoplastic composites. The first results of the implementation of the proposed method into an existing finite element code are shown. Comparison with experimental results is currently under study. The technique described in this study is believed to show great promise for the future as a helpful tool to study the manufacturing of long, discontinuous fiber reinforced thermoplastics and, possibly, continuous fiber systems. Future studies will include the extension of this work to the case of multidirectional laminates as well as the adoption of the more accurate models for the constitutive equation.

A closed form elasticity solution can be used to solve for the stresses and displacements in a heterogeneous anisotropic curved beam loaded in pure bending. The elasticity analysis, based on the superposition of several two-dimensional solutions, provides results which are in very good agreement with those found from mechanics of materials and finite element analysis. The effect of radial heterogeneity on curved beams loaded in pure bending depends on the geometry of the beam. The maximum stress and deflection in beams with a small average radius to depth ratio is significantly effected by heterogeneous material properties. It is unlikely, however, that radial heterogeneity effects the elastic behavior of most beams used in transport aircraft fuselage

580

applications since they have an R/t > 10; but this heterogeneity could play a part in the failure behavior.

The Rayleigh-Ritz analysis can be used to solve problems with both radial and tangential heterogeneity. Stress concentrations can develop which are a function of both the material properties and the heterogeneity. This type of analysis is currently being used to study the effect of heterogeneity on curved beams subject to several different loading conditions: pure bending, internal and external pressure, and end loading. Geometric heterogeneity, such as a notch or cut-out, is also under investigation.

A damage zone mechanics analysis is being developed to study the failure response of structures where heterogeneous material property fields are present as a result of the manufacturing procedures. This model is theoretically based and only requires knowledge of the unnotched strength and fracture toughness of the material to predict failure near a stress concentration.

These models together can be used to establish the relationship between manufacturing and component performance for a variety of forming methods used in thermoplastic composite part production.

## References

1. I. Y. Chang and J. F. Pratte, "LDF Thermoplastic Composites Technology," J. Thermoplastic Comp. Mat., Vol. 4, (1991), pp. 227-252.

2. A. B. Metzner, "Rheology of Suspensions in Polymeric Liquids," J. of Rheology, Vol. 29 (6), (1985), pp. 739-775.

3. T. G. Rogers, "Rheological Characterization of Anisotropic Materials," Composites, Vol. 20, No. 1, (1989), pp. 21-27.

4. P. J. Carreau, "Rheological Equations from Molecular Network Theories," Trans. Soc. Rheol., 16 (1), pp. 99-127 (1972).

5. D. M. Binding, "Capillary and Contraction Flow of Long (Glass) Fiber Filled Polypropylene," Presented at Flow Processes in Composite Materials, University College Galway (Ireland), July 4-5, (1991).

6. O. C. Zienkiewicz and P. N. Godbole. Flow of plastic and viscoplastic solids with special reference to extrusion and forming processes. International Journal for Numerical Methods in Engineering, 8:3-16, 1974.

7. O. C. Zienkiewicz. The Finite Element Method. McGraw-Hill, London, third edition, 1977.

8. E. Oñate and O. C. Zienkiewicz. A viscous shell formulation for the analysis of thin sheet forming. International Journal of Mechanical Science, 25(5):305-335, 1983.

9. A. J. Beaussart. Numerical Modeling of Sheet Forming Processes for Thermoplastic Composites. Master's Degree thesis, Department of Mechanical Engineering, University of Delaware, August 1990.

10. J.F. Pratte, W.H. Krueger, and I.Y. Chang. High Performance Thermoplastic Composites With Poly Ether Ketone Ketone Matrix. 34th International SAMPE Symposium and Exhibition, Reno, NV, May 8-11, 1989.

11. R.B. Pipes, M.H. Santare, B.J. O'Toole, A.J. Beaussart, D.C. DeHeer, and R.K. Okine. Long Discontinuous Fiber Composite Structure - Forming and Structural Mechanics. Proceedings of the First NASA Advanced Composites Technology Conference, Seattle, Washington, Oct. 29-Nov. 1, 1990, pp. 247-270. NASA CP-3104.

12. S. Medwin. Long Discontinuous Ordered Fiber Structural Parts. 34th International SAMPE Symposium and Exhibition, Reno, NV, May 8-11, 1989.

13. S.G. Lekhnitskii. Theory of Elasticity of an Anisotropic Body. Mir Publishers, 1981.

14. S.G. Russell. A Rayleigh-Ritz Analysis Methodology for Cutouts in Composite Structures. Proceedings of the First NASA Advanced Composites Technology Conference, Seattle, Washington, Oct. 29-Nov. 1, 1990, pp. 901-920.

15. Waddoups, M. E., J. R. Eisenmann and B. E. Kaminski. Macroscopic Fracture Mechanics of Advanced Composite Materials. J. of Composite Materials, Vol. 5, pp. 446-454, 1971.

16. Whitney, J. M. and R. J. Nuismer. Stress Fracture Criteria for Laminated Composites Containing Stress Concentrations. J. of Composite Materials, Vol. 8, pp. 253-265, 1974.

17. Nuismer, R. J. and J. M. Whitney. Uniaxial Failure of Composite Laminates Containing Stress Concentrations. In Fracture Mechanics of Composites, ASTM STP 593, pp. 17-142, 1975.

18. Nuismer, R. J. and J. D. Labor. Applications of the Average Stress Criterion: Part I - Tension. J. of Composite Materials, Vol. 12, pp. 238-249,1978.

19. Nuismer, R. J. and J. D. Labor. Applications of the Average Stress Criterion: Part II - Compression. J. of Composite Materials, Vol. 13, pp. 49-60,1979.

20. J. Backlund. Fracture Analysis of Notched Composites. Computers and Structures, Vol. 13, pp. 145-154, 1981.

21. Backlund, J. and C-G. Aronsson. Tensile Fracture of Laminates With Holes. J. of Composite Materials, Vol. 20, pp. 259-286, 1986.

22. Aronsson, C-G. and J. Backlund. Tensile Fracture of Laminates With Cracks. J. of Composite Materials, Vol. 20, pp. 287-307, 1986.

| Term | Newtonian | Power-Law | Carreau |
|---|---|---|---|
| $\eta_{11}$ | $\frac{\eta f}{2}[\kappa-1](L/D)^2$ | $2^m\eta f[\kappa-1]^m(L/D)^{(m+1)}(\dot{\varepsilon}_{11})^{(m-1)}$ | $\frac{\eta_0 A_T(\kappa-1)f}{2}(L/D)^2\left[1+\frac{A_T^2(\kappa-1)^2(L/D)^2}{4}(\lambda\dot{\varepsilon}_{11})^2\right]^{(n-1)/2}$ |
| $\eta_{12}$ | $\kappa\eta$ | $\eta\,\kappa^m(\dot{\gamma}_{12})^{(m-1)}$ | $\eta_0 A_T\kappa\,[1+(A_T\lambda\kappa)^2(\dot{\gamma}_{12})^2]^{(n-1)/2}$ |
| $\eta_{23}$ | $\kappa\eta$ | $\eta\,\kappa^m(\dot{\gamma}_{23})^{(m-1)}$ | $\eta_0 A_T\kappa\,[1+(A_T\lambda\kappa)^2(\dot{\gamma}_{12})^2]^{(n-1)/2}$ |
| $\eta_{22}$ | $4\kappa\eta$ | $2^{(m+1)}\eta\,\kappa^m(\dot{\varepsilon}_{22})^{(m-1)}$ | $4\eta_0 A_T\kappa\,[1+(A_T\lambda\kappa)^2(\dot{\varepsilon}_{22})^2]^{(n-1)/2}$ |

Table 1. Anisotropic viscosities for long discontinuous fiber thermoplastic composites
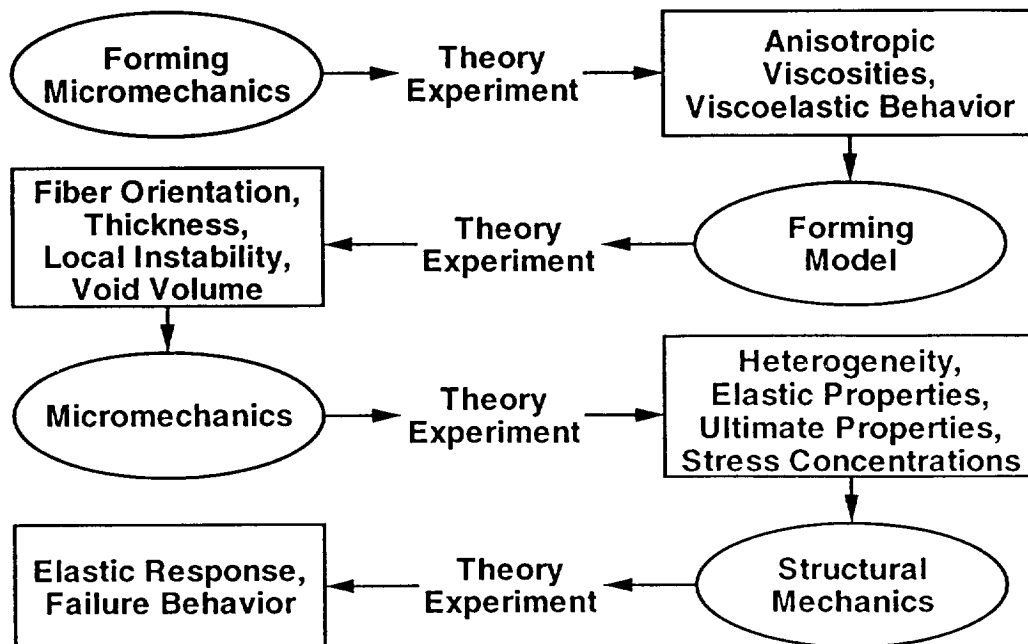


Figure 1. Summary of research plan
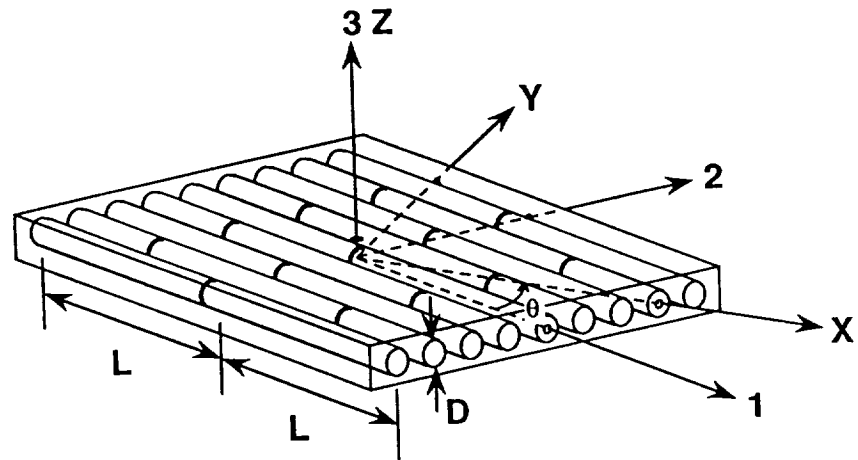
Figure 2. Oriented fiber assembly
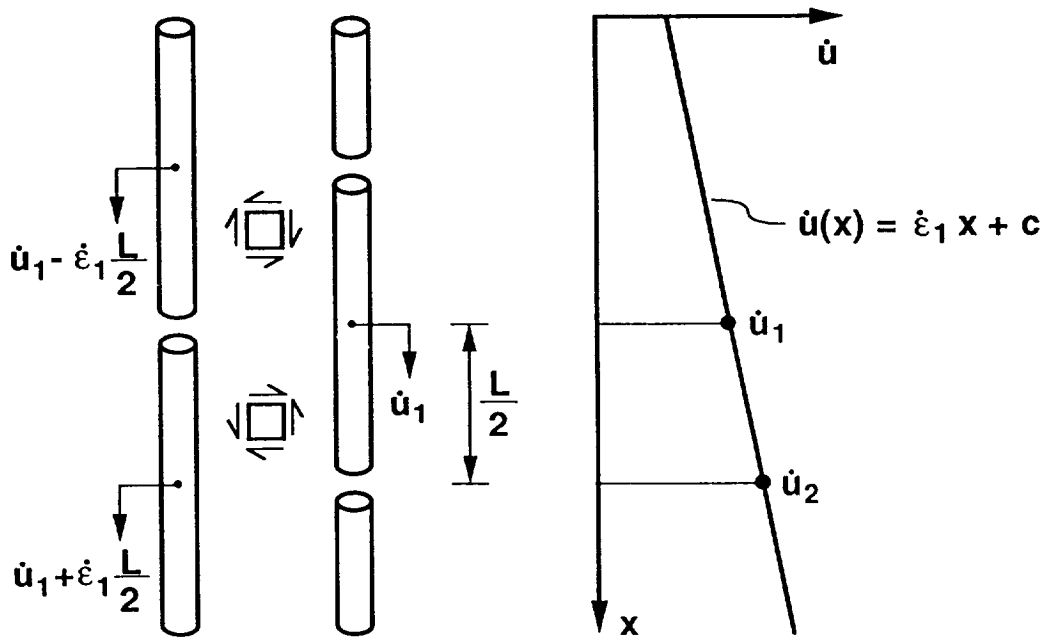


Figure 3. Fiber kinematics in extension
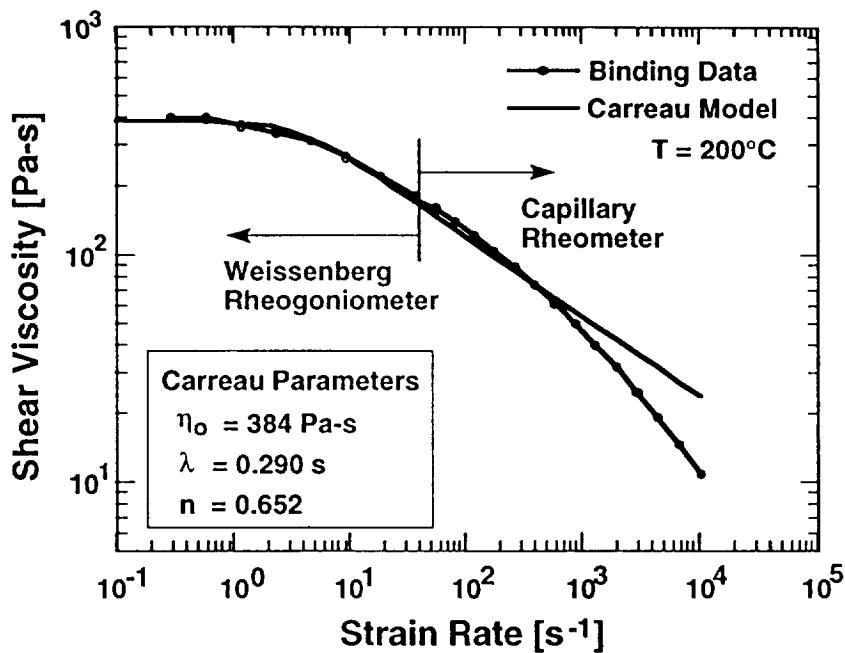
Figure 4. Shearing viscosity vs. strain rate for polypropylene, Binding data and Carreau fit
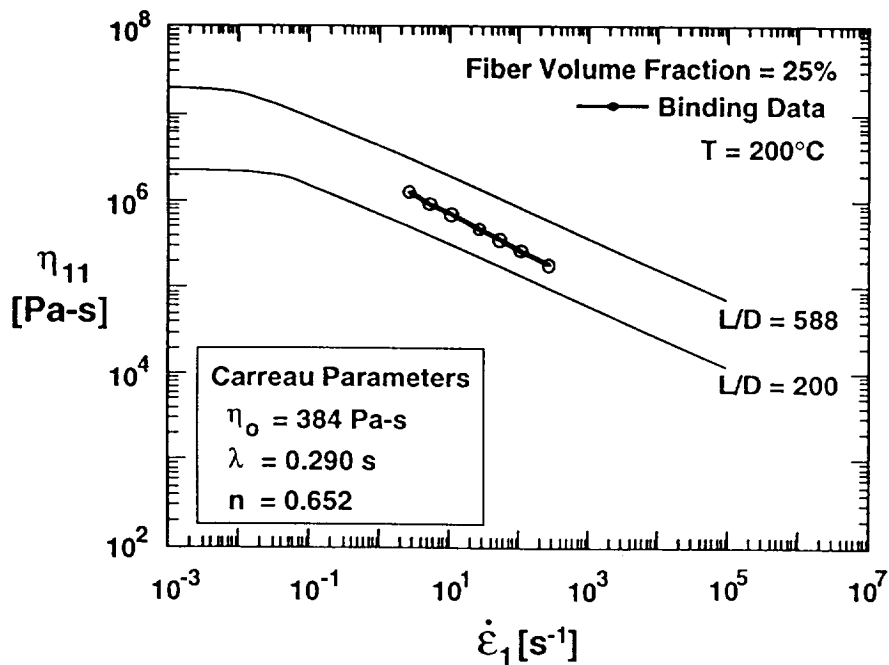


Figure 5. Elongational viscosity vs. strain rate for glass fiber polypropylene
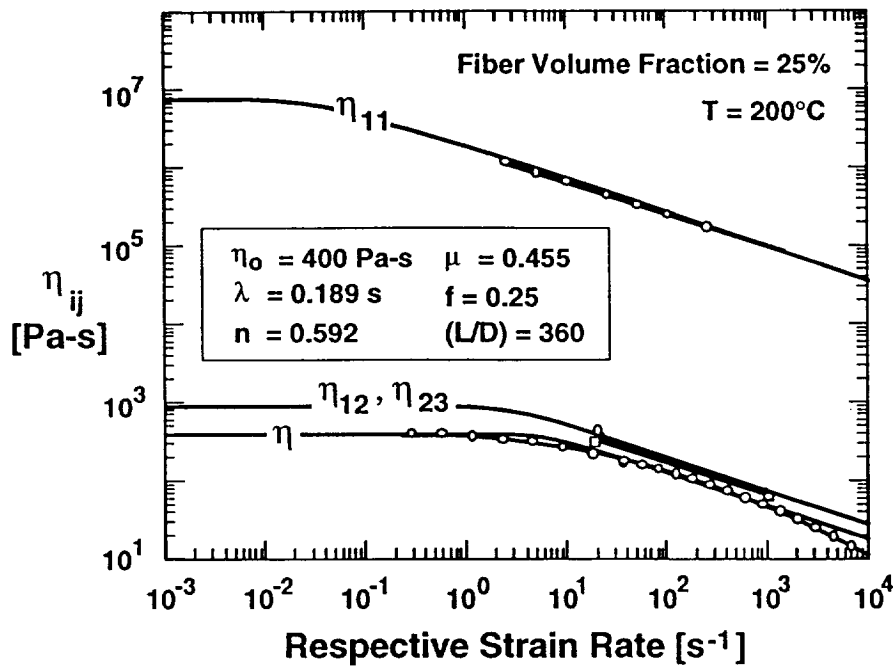
Figure 6. Comparison between predicted and experimentally measured viscosities
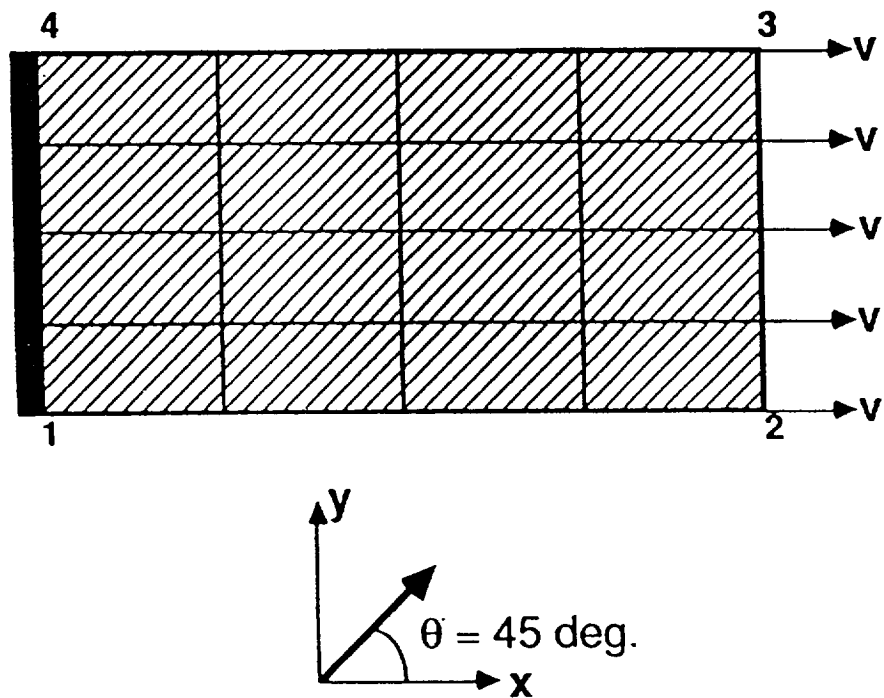


Figure 7. Off axis tensile test, initial geometry of finite element simulation

586

C-2

step #2

step #4

step #8

step #12

step #16

step #20
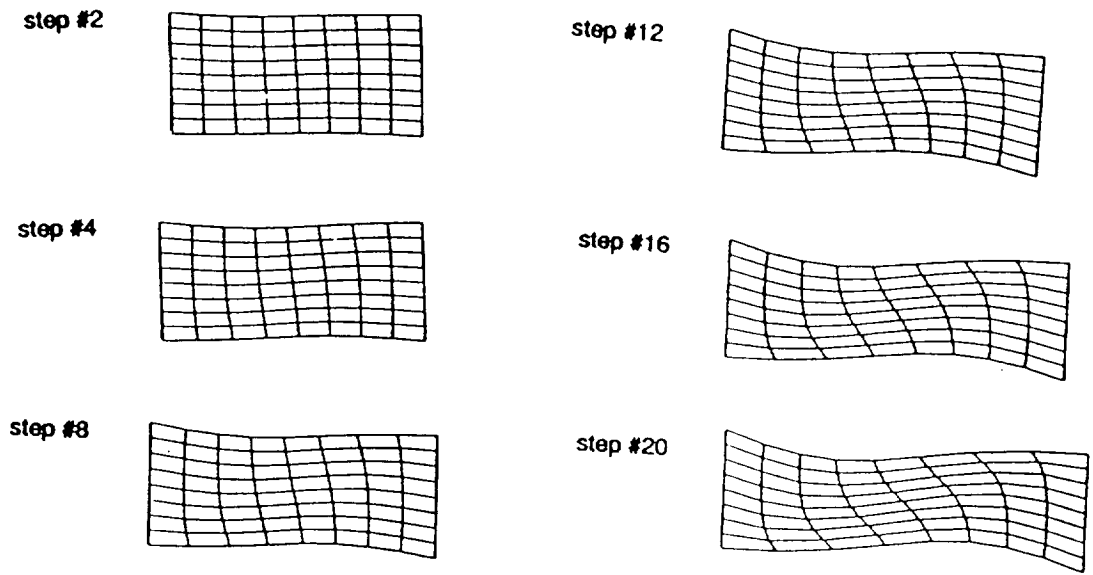
Figure 8. Several stages of the simulated deformation

step #2

step #4

step #8

step #12

step #16

step #20
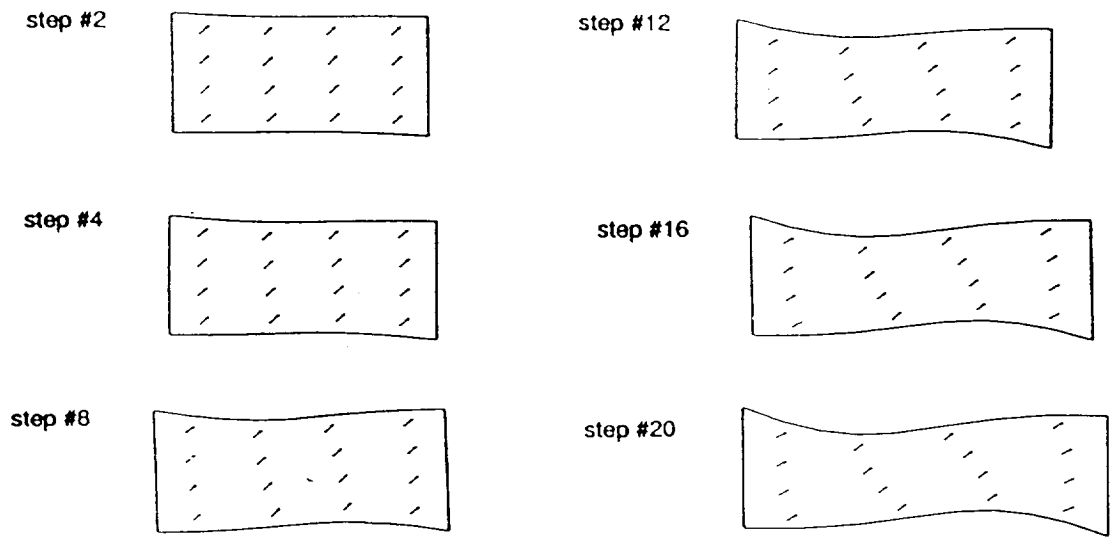
Figure 9. Fiber orientation during simulated deformation
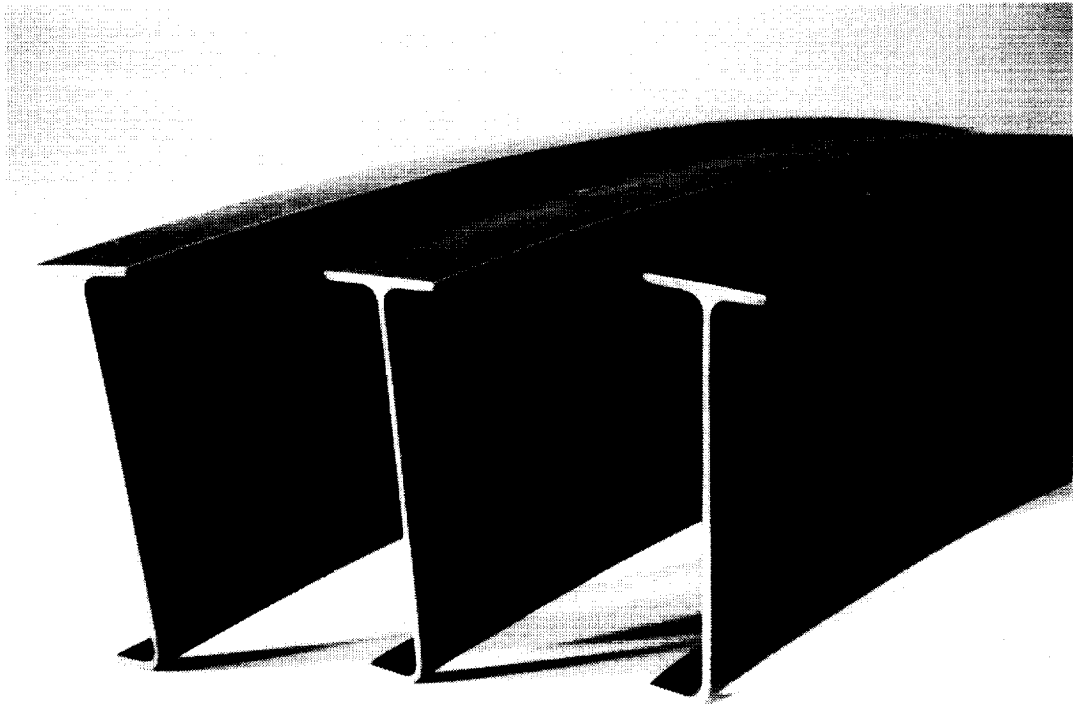
Figure 10. Thermoplastic composite curved beams
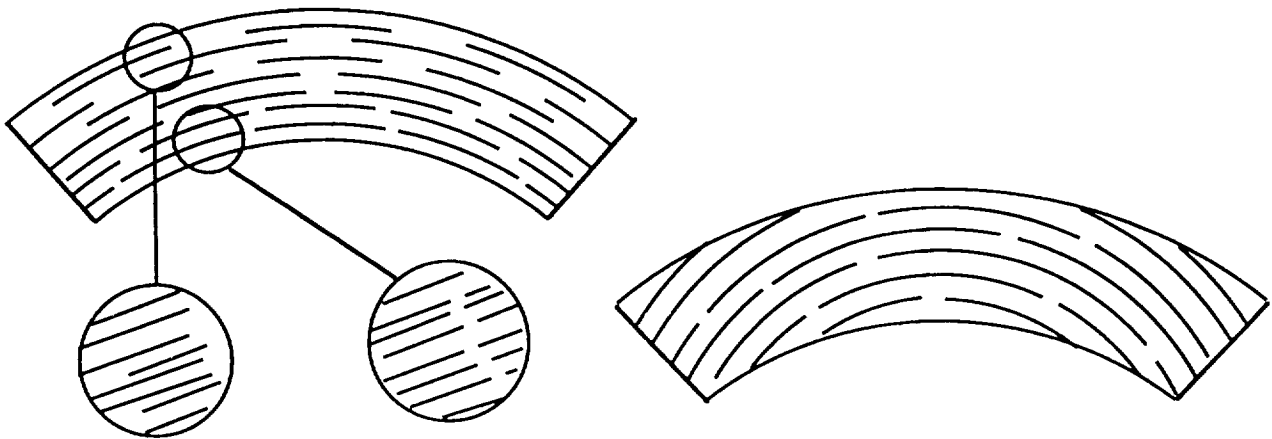


Figure 11. Different types of possible material heterogeneity

**Lines of Constant Tangential Stress, Units in psi.**
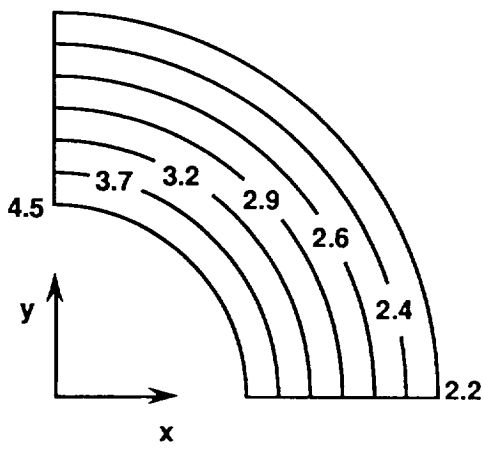


A. Tangentially Oriented Fibers
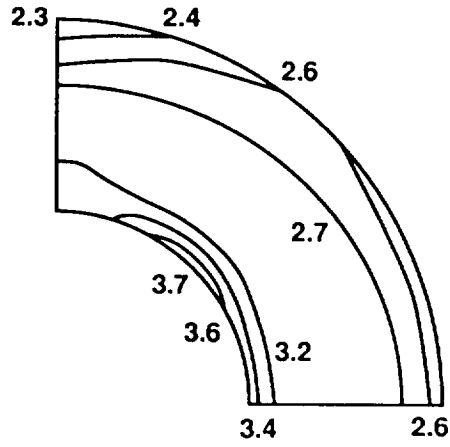
B. Fibers Oriented In X-Direction

Figure 12. Tangential stress contours in a circular ring loaded by internal pressure
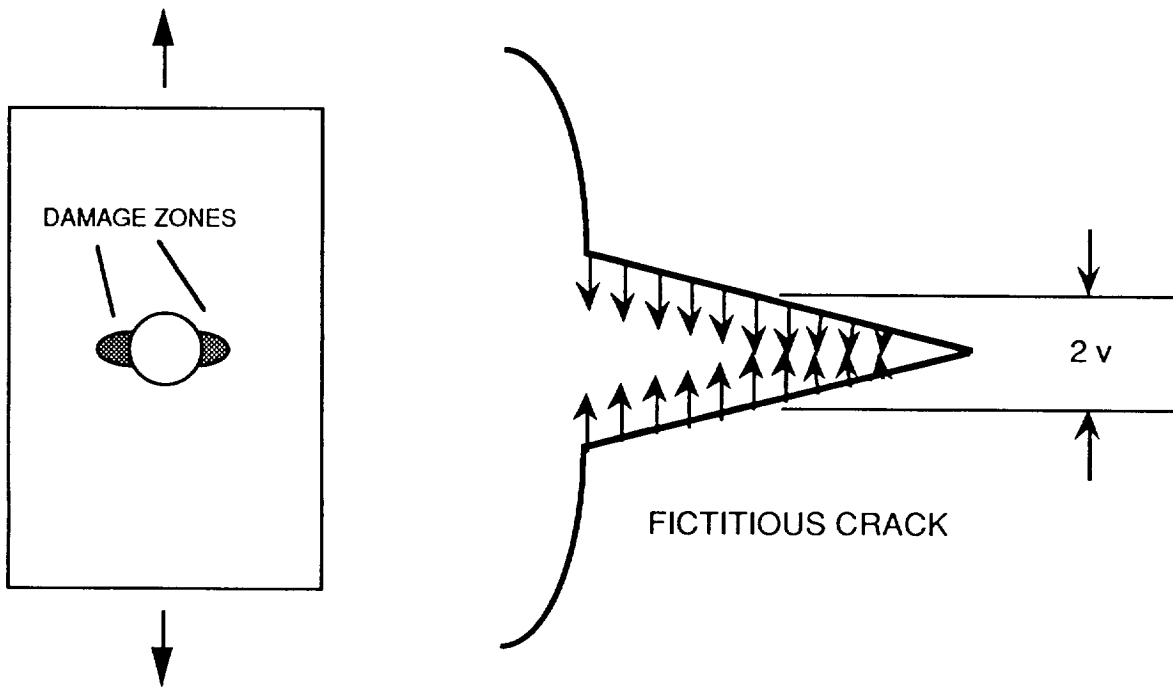


Figure 13: Damaged zone represented by fictitious crack

589
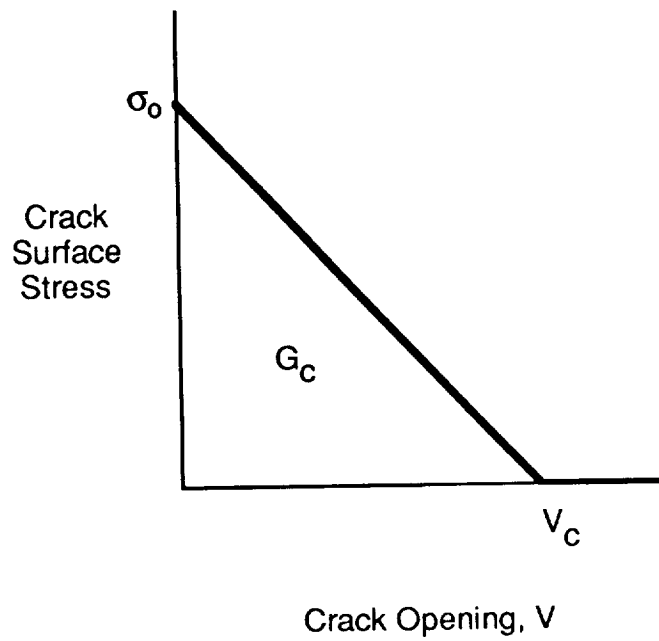
Figure 14: Crack surface stress vs. crack opening
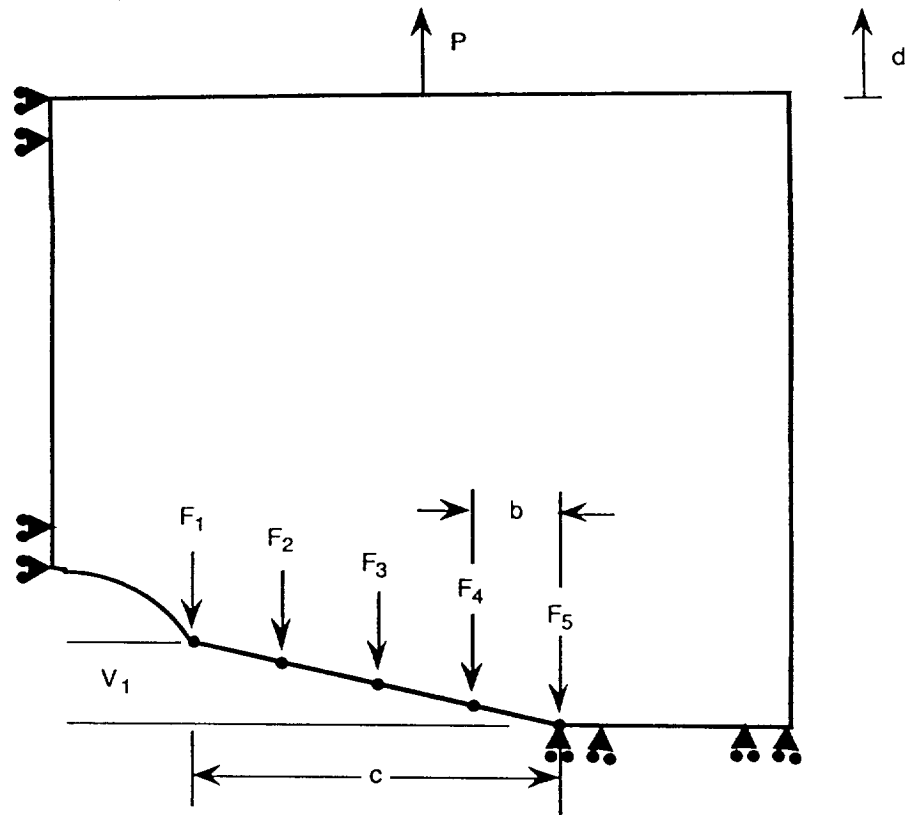


Figure 15: Plate geometry and computational parameters